WILEY-VCH

Günther Rüdiger, Leonid L. Kitchatinov,
Rainer Hollerbach

Magnetic Processes in Astrophysics

Theory, Simulations, Experiments

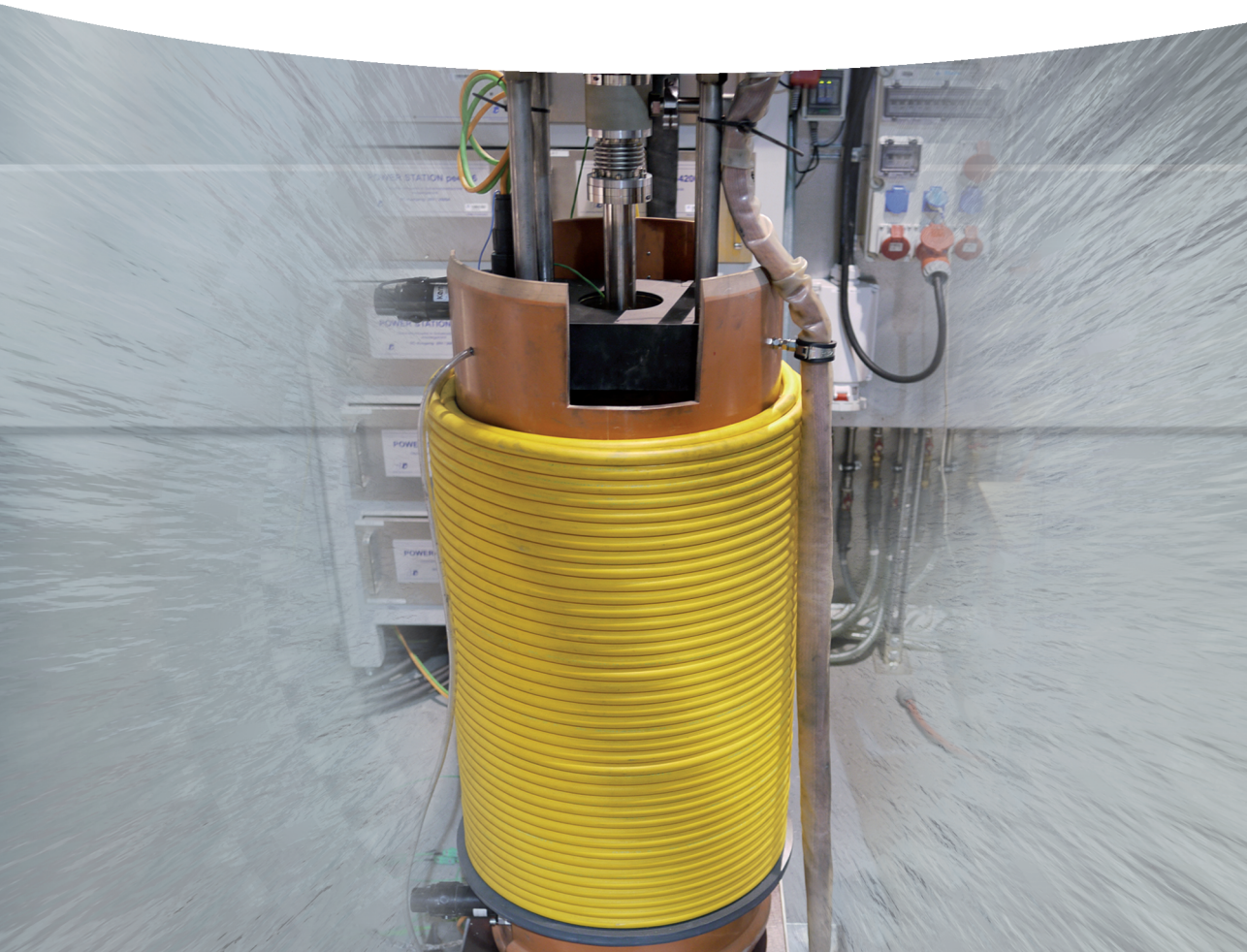

Günther Rüdiger,
Leonid L. Kitchatinov, and
Rainer Hollerbach

Magnetic Processes in Astrophysics

Related Titles

McCarthy, D.D., Seidelmann, P.K.

Time – From Earth Rotation to Atomic Physics

2009
ISBN: 978-3-527-40780-4

Sidorenkov, N.S.

The Interaction Between Earth's Rotation and Geophysical Processes

2009
ISBN: 978-3-527-40875-7

Shore, S.N.

Astrophysical Hydrodynamics
An Introduction

2007
ISBN: 978-3-527-40669-2

Stahler, S.W., Palla, F.

The Formation of Stars

2004
ISBN: 978-3-527-40559-6

Foukal, P.V.

Solar Astrophysics

2004
ISBN: 978-3-527-40374-5

Spitzer, L.

Physical Processes in the Interstellar Medium

1998
ISBN: 978-0-471-29335-4

Günther Rüdiger, Leonid L. Kitchatinov,
and Rainer Hollerbach

Magnetic Processes in Astrophysics

Theory, Simulations, Experiments

WILEY-VCH
Verlag GmbH & Co. KGaA

The Authors

Prof. Günther Rüdiger
Leibniz-Institut für Astrophysik Potsdam (AIP)
An der Sternwarte 16
14482 Potsdam
Germany

Dr. Leonid L. Kitchatinov
Institute for Solar-Terrestrial
Physiks
Lermontov st., 126 a
664033 Irkutsk
Russian Federation

Prof. Rainer Hollerbach
Institut für Geophysik
ETH Zürich
8092 Zürich
Switzerland

Cover Picture
The PROMISE facility for experimental studies of the helical and the azimuthal magnetorotational instability, constructed and operated at Helmholtz-Zentrum Dresden-Rossendorf.

Library of Congress Card No.:
applied for

British Library Cataloguing-in-Publication Data:
A catalogue record for this book is available from the British Library.

Bibliographic information published by the Deutsche Nationalbibliothek
The Deutsche Nationalbibliothek lists this publication in the Deutsche Nationalbibliografie; detailed bibliographic data are available on the Internet at http://dnb.d-nb.de.

Print ISBN 978-3-527-41034-7
ePDF ISBN 978-3-527-64895-5
ePub ISBN 978-3-527-64894-8
mobi ISBN 978-3-527-64893-1
oBook ISBN 978-3-527-64892-4

Cover Design Grafik-Design Schulz, Fußgönheim
Typesetting le-tex publishing services GmbH, Leipzig
Printing and Binding Markono Print Media Pte Ltd, Singapore

Printed in Singapore

Printed on acid-free paper

Contents

Preface

In 2004 two of us (Rüdiger and Hollerbach) published a previous book entitled *The Magnetic Universe: Geophysical and Astrophysical Dynamo Theory*, describing the origin of magnetic fields in objects ranging in size from planets to galaxies. Ever since then, we have considered the possibility of writing a second edition, updating developments of the past decade. However, ultimately there were so many recent developments in areas not covered at all before that it ended up as a completely new book, with only minimal overlap (in parts of Chapters 1 and 4) with corresponding formulations in Rüdiger and Hollerbach (2004). In particular, the subjects of these two chapters (differential rotation theory, the galactic dynamo) have developed so rapidly since then that a new discussion was clearly necessary.

On the one hand, the successful asteroseismic space missions MOST, CoRoT and KEPLER ushered in a new era of knowledge of the internal stellar rotation laws. Stars exhibit much greater variety of turbulent convection zones and angular momentum than found in the Sun, so that it is now possible to develop the theory of the rotation of stars by means of the new data. It is also clear that only facts about stellar differential rotation allow us to understand the magnetic activity of the main-sequence stars.

On the other hand, the interstellar medium forms one of the most impressive realizations of driven cosmical turbulence under the influence of a (nonuniform) rotation, where both can be observed *in situ*. Observers find a strong stratification in the vertical direction of gas and turbulence, hence large-scale helicity should exist. In such cases mean-field dynamo theory predicts the instability of the solution $\boldsymbol{B} = \boldsymbol{0}$ and consequently the existence of large-scale magnetic fields which can also be observed. The correctness of this scenario has been successfully probed with numerical simulations which are presented here as a convincing instance of the state of the modern dynamo theory.

One significant change though from Rüdiger and Hollerbach (2004) is the switch in emphasis from being primarily on dynamo theory more toward magnetic instabilities such as the magnetorotational instability or the Tayler instability. That is, instead of seeking to explain the origin of magnetic fields, we now take the existence of large-scale fields as given, and study the ways in which instabilities can destroy the large-scale structures again, and give rise to small-scale turbulence instead.

Another aspect that has changed significantly since 2004 is the increasing importance of liquid metal (and plasma) laboratory experiments, not only in attempts to create laboratory dynamos, but also involving externally imposed magnetic fields. In addition to the chapters on the magnetorotational and Tayler instabilities, the chapter on magnetic spherical Couette flow describes a number of new experiments. In all of these areas, the interplay between basic theory, detailed numerical simulations, and experiments has been particularly fruitful, with generally good agreement also between theory and experiment (perhaps "disappointingly" good, if one views unexpected experimental results as the ones most likely to further lead to fundamentally new insights). At any rate, we hope that this book will be of interest not just to astrophysicists but to fluid dynamicists more generally, or anyone else wanting to understand liquid metal experiments and the insights they can yield.

Numerous colleagues have contributed to this book, either directly or by general discussions over many years. GR particularly thanks Rainer Arlt, Detlef Elstner, Marcus Gellert, Andrea Hans, Manfred Küker and Manfred Schultz of the Leibniz-Institut für Astrophysik Potsdam for their substantial support with countless technical details. LLK and GR acknowledge the continuous encouragement of the Deutsche Forschungsgemeinschaft and the Alexander von Humboldt Foundation stimulating a number of the developments presented here. RH thanks Prof Andy Jackson of the Institute of Geophysics at ETH Zürich for the invitation to visit ETH (with funding by the European Research Council). The time away from regular duties was invaluable in finishing this project in time. Finally, among the vast MHD community we particularly thank Gunter Gerbeth, Thomas Gundrum, Martin Seilmayer, Frank Stefani and the entire group at the Helmholtz-Zentrum Dresden-Rossendorf for many intensive discussions and collaborations over the past decade, as presented in several of the chapters here, and which we hope may stimulate further developments in MHD laboratory astrophysics.

Potsdam — *Günther Rüdiger*
Irkutsk — *Leonid L. Kitchatinov*
Zürich — *Rainer Hollerbach*
2013

1
Differential Rotation of Stars

Magnetic activity of solar-type stars is closely related to stellar rotation. The differential rotation participates in stellar dynamos by producing toroidal magnetic fields by rotational shear. Differential rotation and meridional flow can be understood in the context of mean-field hydrodynamics in stellar convection zones. Stratification in convection zones is so strong that the Schwarzschild criterion ($\mathrm{d}S/\mathrm{d}r < 0$, where S is the specific entropy) is fulfilled and the entire zone becomes turbulent. Due to the radial stratification the turbulence fields are themselves stratified with the radial preferred direction. Interaction of such a turbulence with an overall rotation leads to the formation of large-scale structure. Lebedinskii (1941), Wasiutynski (1946), Biermann (1951) and Kippenhahn (1963) were the first to find that differential rotation and meridional flow might be direct consequences of the rotating anisotropic turbulence. Details of the long history of this concept were presented by Rüdiger (1989, Chapter 2).

Whether a star is of solar-type is controlled by its structure. Stars of this type possess external (turbulent) convection zones. The solar convection zone only includes $< 2\%$ of the total mass ($M_\odot$) but it extends about 30% in radius. The outer convection zones in cooler stars become deeper as stellar mass decreases until for M stars the convection zone reaches down to the center. On the other hand, for A stars the outer convection zone becomes very thin, but an inner zone becomes convectively unstable. For B stars this inner convection zone reaches considerable dimensions.

The level of stellar activity depends strongly on spectral type. There is, however, the striking fact that the linear depth of the outer convection zone, at 200 000 km, does not vary too much among the solar-type stars. We shall see later how important the total thickness of a convection zone is for the formation of differential surface rotation.

It is certainly unrealistic to expect a solution of the complicated problem of stellar dynamos if the internal stellar rotation laws cannot be predicted or observed (by asteroseismology). Differential rotation is explained here as turbulence-induced with only a small magnetic contribution. Mean-field hydrodynamics provides a theoretical basis for differential rotation modeling, so that the models can be constructed with very little arbitrariness. Nevertheless, differential rotation of the Sun can be re-

Magnetic Processes in Astrophysics, First Edition. G. Rüdiger, L.L. Kitchatinov, and R. Hollerbach.

produced by computations very closely and the dependence of differential rotation on stellar parameters can be predicted.

1.1 Solar Observations

1.1.1 The Rotation Law

The rotation of the solar photosphere was measured using the Doppler shifts of photospheric spectral lines or tracking rotation of sunspots and various other tracers. Doppler measurements of Howard *et al.* (1983) and the classical work of Newton and Nunn (1951) on sunspot rotation are the well-known examples. Within a small percentage, all measurements yield similar results. Obtained by tracing bright coronal structures in SOHO images Wöhl *et al.* (2010) give

$$\Omega = 0.253 - 0.044 \sin^2 b - 0.013 \sin^4 b \quad [\text{rad/day}] \tag{1.1}$$

for the sidereal rotation rate, with $b = 90° - \theta$ as the heliographic latitude. The angular velocity of 0.25 rad/day leads to a frequency of 462 nHz at the equator. The observed equator–pole difference of the angular velocity, $\delta\Omega$, from (1.1) is 0.057 rad/day. We shall characterize the existence of differential rotation by the quantity $\delta\Omega = \Omega_{\rm eq} - \Omega_{\rm pole}$ rather than by the ratio

$$\mathrm{k} = \frac{\Omega_{\rm eq} - \Omega_{\rm pole}}{\Omega_{\rm eq}} \tag{1.2}$$

(here ≈ 0.23) because only $\nabla\Omega$ is relevant for the inducting action of differential rotation but not its normalized value k. With (1.2) we follow the notation of the seminal paper by Hall (1991) who derived from photometric stellar observations a relation $\mathrm{k} \propto \Omega^{-0.85}$ (corresponding to the very flat relation $\delta\Omega \propto \Omega^{0.15}$ for rotating stars, see also Barnes *et al.* (2005)) which is rather close to the essentials presented in the theoretical part of this chapter.

Brown (1985) made the first attempt to infer how the latitudinal differential rotation varies with depth from rotational splitting of frequencies of global acoustic oscillations. Today the helioseismological inversions provide a detailed portrait of the internal solar rotation (Wilson, Burtonclay, and Li, 1997; Schou *et al.*, 1998). Figure 1.1 shows the distribution of rotation rate inside the Sun. Latitudinal differential rotation seen on the solar photosphere survives throughout the convection zone up to its base. Helioseismology detects the location of the inner boundary of the convection zone at $r_{\rm in} = 0.713\, R_\odot$ (Christensen-Dalsgaard, Gough, and Thompson, 1991; Basu and Antia, 1997). Latitudinal differential rotation at the inner boundary is reduced about twice compared with the surface (Charbonneau *et*

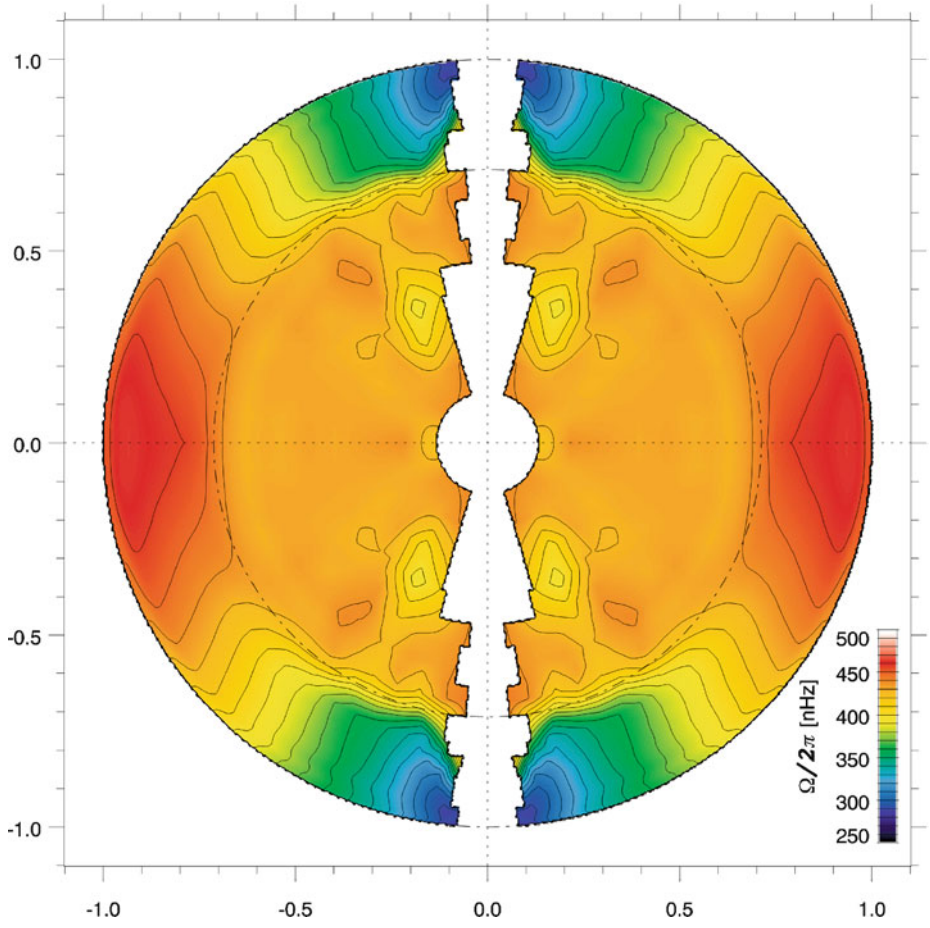

Figure 1.1 Isolines of the angular velocity of the Sun after Korzennik and Eff-Darwich (2011). The rotation of the polar and the near-center regions is difficult to measure. With permission of the authors.

al., 1999). A remarkable feature of Figure 1.1 is the sharp transition from differential to rigid rotation in a thin layer near the base of the convection zone. This layer, called after Spiegel and Zahn (1992) the solar "tachocline," extends not more than 4% in radius (Kosovichev, 1996; Antia, Basu, and Chitre, 1998). Its midpoint is at $(0.692 \pm 0.005)\ R_\odot$, and it is slightly prolate in shape (Charbonneau *et al.*, 1999). The tachocline is, therefore, located mainly if not totally beneath the base of the convection zone, in the uppermost radiative zone. Rotation beneath the tachocline is almost rigid at least down to $0.2\ R_\odot$ (Couvidat *et al.*, 2003; Korzennik and Eff-Darwich, 2011).

The main empirical features of the solar differential rotation can be summarized as follows (see Figure 1.1):

- an equatorial acceleration of about 23% at the surface,
- a near-surface shear layer with negative Ω-gradient in radius[1)],
- a sharp transition to rigid rotation in a thin tachocline,
- a rigid rotation of the deeper radiative core.

The 'observed' phenomenon of the sharp transition layer between the outer domain of differential rotation and the inner domain of rigid-body rotation is hard to understand without the assumption of internal empirically unknown magnetic fields. We shall show in Section 2.2 that indeed fossil fields with amplitudes of only 1 mG are enough to explain not only the existence of the tachocline but also its small radial extension.

The present state of differential rotation may, however, differ from other epochs when magnetic activity of the Sun was different. Ribes and Nesme-Ribes (1993) used statistics of sunspot observations over the Maunder minimum at the Observatoire de Paris to find a rotation rate slower by about 2% at the equator and by about 6% at midlatitudes than at the present time. The differential rotation was thus stronger than today. The more magnetic the Sun, the faster and more rigidly its surface rotates. Balthasar, Vázquez, and Wöhl (1986), however, could not find similar results for a regular minimum. Also Arlt and Fröhlich (2012), who worked with data obtained from the drawings of Staudacher from the period from 1749 till 1799 did not find a significant difference to the present-day value of $\delta\Omega \simeq 0.050$ rad/day derived by Balthasar, Vázquez, and Wöhl (1986) from sunspot rotation. The reported average value of 0.048 indicates a slightly smaller value but this difference is not yet significant.

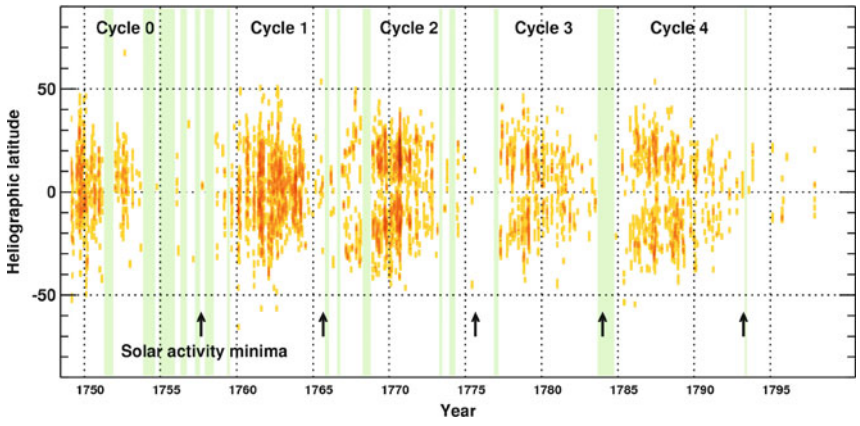

Figure 1.2 The butterfly diagram shortly after the Maunder minimum, as derived from the drawings of Staudacher between 1749 and 1799. Courtesy of R. Arlt.

1) Young spots rotate faster by about 4% than the solar surface plasma, see (1.37).

The results are nevertheless highly interesting as they demonstrate the reliability of the data which also led to the construction of a butterfly diagram for the four cycles covered by the observations. The main question here is whether the dipolar parity which now dominates the solar activity already existed shortly after the Maunder minimum. This is certainly the case for the last two cycles shown in Figure 1.2 but it seems to be questionable for the older two cycles. For these cycles, which are closer to the Maunder minimum at least an overpopulation of near-equator sunspots is indicated by the data (Arlt, 2009).

1.1.2 Torsional Oscillations

As magnetic activity of the Sun varies with time, differential rotation may also be expected to be time-dependent. Variations of solar rotation law are indeed observed. Schrijver and Zwaan (2000), Stix (2002) and Thompson *et al.* (2003) presented detailed historical and data-based overviews of all phenomena concerning the temporal variations of the solar rotation law. As the magnetic force is quadratic in the magnetic field, the resulting flow is expected to vary with twice the frequency of the 22-year magnetic cycle. The 11-year torsional oscillations were first observed by Howard and LaBonte (1980).

Figure 1.3 shows the oscillation pattern. At a fixed latitude there is an oscillation of fast and slow rotation with an 11-year period. The whole pattern migrates at about 2 m/s toward the equator. The migration follows the equatorial drift of magnetic activity. Latitudinal shear of differential rotation is increased in the activity belt with faster than average rotation on the equatorial side of the belt and slower than average rotation on the polar side. Howe, Komm, and Hill (2002) showed by helioseismological inversions that the migrating torsional oscillation exists not

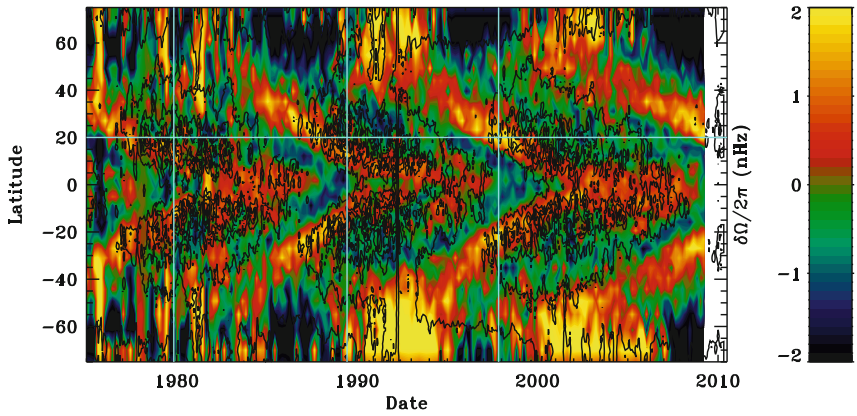

Figure 1.3 Torsional oscillations derived from Doppler shift measurements. The flow pattern follows the equatorial drift of magnetic activity. The flow at a given latitude oscillates with a period of about 11 years. Courtesy of Howe *et al.* (2011).

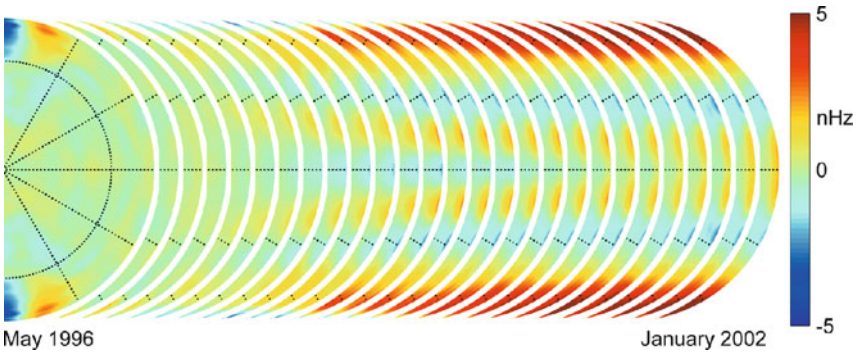

Figure 1.4 Helioseismology detects two branches of torsional oscillations migrating to the equator and to the poles from midlatitude and extending deep into the convection zone. From Vorontsov *et al.* (2002). Reprinted with permission from AAS.

only at the surface, but that it extends at least 60 000 km down into the convection zone.

An important question of dynamo theory is whether a poleward migrating branch is present at high latitudes. Schou (2001) and Vorontsov *et al.* (2002) reported the detection of such a branch of torsional oscillation for the rising phase of solar cycle 23 from helioseismological data between 1996 and 2002. Figure 1.4 shows the polar branch together with the low-latitude equatorial branch penetrating deep into the convection zone.

Close correlation with solar activity is indicative of a magnetic origin of torsional oscillations. Details of the mechanism producing the oscillations remain, however, uncertain. The oscillations may be produced by the global Lorentz force (Yoshimura, 1981; Schüssler, 1981; Rüdiger *et al.*, 1986) or the magnetic backreaction on small spatial scale of turbulence (Kitchatinov, 1990; Rüdiger and Kitchatinov, 1990). Meridional flow induced by entropy disturbances in the magnetic activity belt may also be relevant (Spruit, 2003; Cameron and Schüssler, 2012).

1.1.3
Meridional Flow

It was recognized since the work of Kippenhahn (1963) that differential rotation and meridional flow are closely related and it is not possible to correctly describe one if the other is not allowed for.

The relatively slow meridional circulation is difficult to measure. Ward (1965) noticed that the flow is problematic to define by the method of tracers: an inhomogeneity of tracer distribution over latitude together with latitudinal turbulent diffusion results in a false meridional flow. This is probably why early measurements using sunspots as tracers gave conflicting results. A more coherent picture is provided by using more uniformly distributed 'small magnetic features' as tracers. Komm, Howard, and Harvey (1993) found a meridional flow from the equator

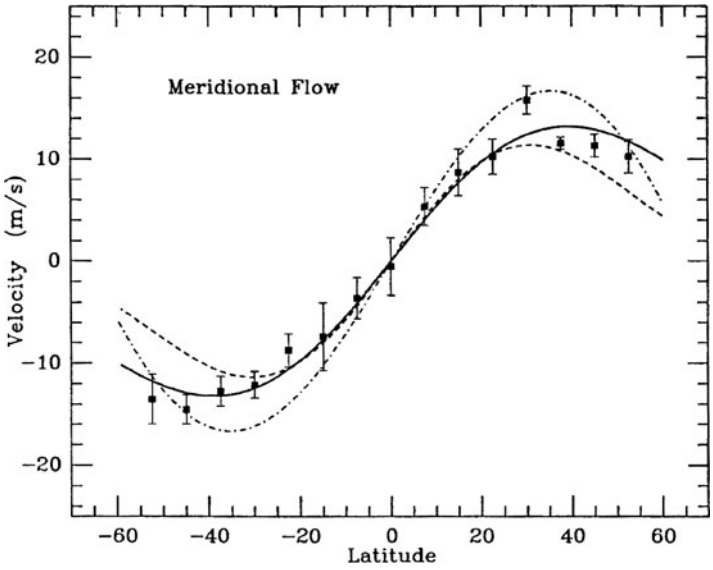

Figure 1.5 Full line and symbols show the meridional flow measured by using small magnetic features as tracers. Overplotted are Doppler measurements of Ulrich (1993) (dashed-dotted) and Snodgrass (1984) (dashed). From Komm, Howard, and Harvey (1993).

to pole with amplitude slightly above 10 m/s. The flow is shown in Figure 1.5. The flow pattern shows no hemispheric asymmetry and did not migrate in latitude during a solar cycle. The amplitude of the flow varies, however, over the activity cycle. Meridional velocity changes from below average during solar maximum to above average during solar minimum. The relative amplitude of the variation is about 25%. This picture is supported by recent measurements of Hathaway and Rightmire (2010) and by seismological sounding of the flow by Basu and Antia (2010).

Zhao and Kosovichev (2004) measured the meridional flow for seven Carrington rotations of years 1996–2002 covering the epoch from solar activity minimum to maximum. The measurements by time-distance helioseismology show the poleward flow decreasing with depth in the surface layer of 12 000 km. In addition to the dominating poleward flow of order 20 m/s, cells of weaker flow converging to the activity belts were found in both hemispheres. These cells migrated towards the equator following the migration of activity belts as the solar cycle evolved. These migrating cells may be a counterpart of torsional oscillations in the meridional flow.

Gizon and Rempel (2008) analyzed MDI data from 1996 to 2002. The resulting surface flow is poleward up to $\pm 50^\circ$ latitude. The flow velocity peaks at about 25°. The peak-to-peak variation in time is, at 7 m/s, rather large. There is no indication for a second (polar) cell of meridional circulation (Figure 1.6). The same is true for the flow at a depth of 60 000 km where the amplitude of the poleward flow is 6 m/s peaking again at 25°. Schad, Timmer, and Roth (2012) even reach $x = 0.8$, that is a

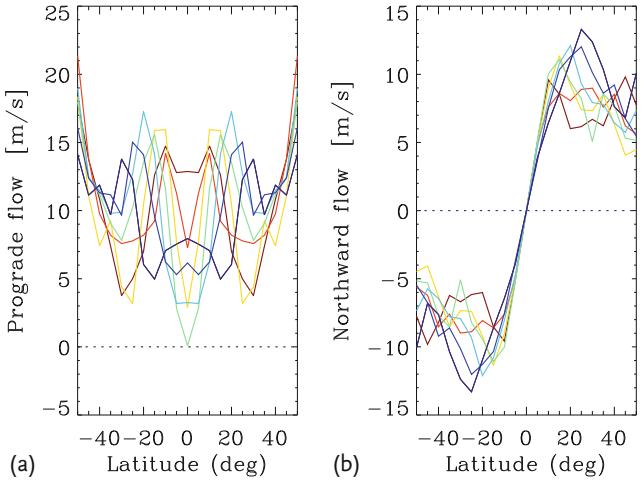

Figure 1.6 Helioseismology results (MDI) for the rotational velocity (a) and meridional flow (b) in their dependencies on latitude and time (from 1996 (blue) to 2002 (red)). The meridional flow is poleward with an amplitude of 10 m/s, which varies in time by 7 m/s. From Gizon and Rempel (2008).

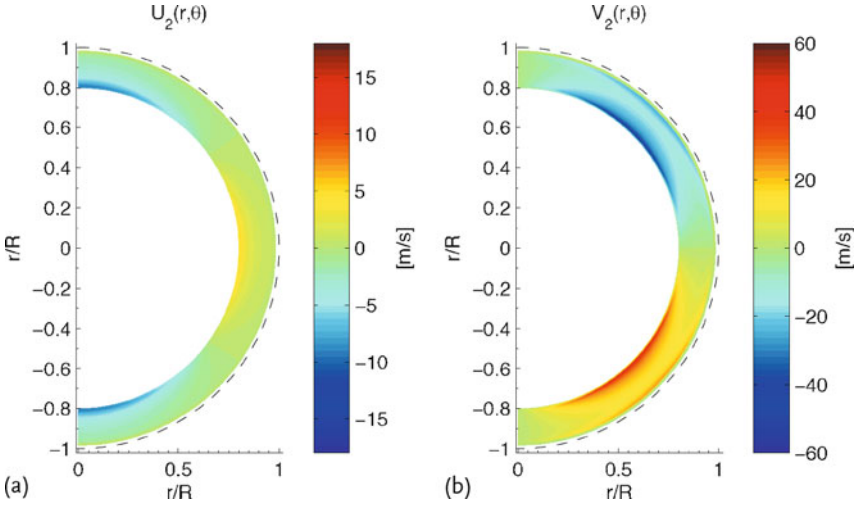

Figure 1.7 Helioseismology results for the radial (a) and the latitudinal (b) components of the meridional flow from the surface down to $x = 0.8$. The latitudinal flow is always poleward while the radial flow is upward at the equator and downward at the poles. Courtesy of M. Roth.

depth of 140 000 km (Figure 1.7). The main conclusion is that indeed only one cell with counterclockwise circulation exists in the solar convection zone, whose return flow exists below $x = 0.8$. This result is of basic significance for both the theory of differential rotation and the theory of the solar dynamo.

The question for the equatorward return flow deep in the convection zone has also been considered by Hathaway *et al.* (2003). From the sunspot data since 1874 they found an anticorrelation between the drift rate of the center of the butterfly diagram and the cycle length. The faster the drift of the butterfly diagram the shorter the cycles. With such statistics an amplitude of 1.2 m/s for the return flow velocity at the bottom of the convection zone has been estimated.

1.2 Stellar Observations

1.2.1 Rotational Evolution

Rotation of a star is an important parameter of hydromagnetic dynamos controlling the rate of magnetic field generation. The dynamo activity in turn decreases the rotation rate. Solar-type stars are observed to exhibit a steady decline in rotation rate between the ages from about 10^8 to 4.5×10^9 years (Skumanich, 1972).

The spin-down is commonly explained as follows (Kraft, 1967): magnetic activity of stars with external convection zones produce hot stellar coronae. Similar to the Sun, the hot coronae emanate stellar winds. The material making up the wind does not lose contact with the parent star after leaving its photosphere, but corotates with the star due to magnetic coupling to its surface. The extent of the coupling can be (very crudely) estimated by the Alfvén radius, R_A, where the wind velocity equals the Alfvén speed. As the angular momentum loss is proportional to R_A^2, magnetic activity enhances the rotational braking. Spindown of the main-sequence dwarfs closely obeys the Skumanich law,

$$P_{\rm rot} \propto \sqrt{t}\,, \tag{1.3}$$

relating rotation period $P_{\rm rot}$ of a star to its age t.

This law does not, however, apply to all stellar ages. Solar mass stars are born with rotation periods of about one week. Subsequently, these stars spin-up very quickly during contraction to the main-sequence to attain a rotation period of about one day or even shorter as ZAMS stars (Hartmann and Noyes, 1987). Close to the end of their main-sequence lives, stars seem to deviate from relation (1.3) as well. Figure 1.8 shows that the upper-left corner on the plot of $P_{\rm rot}$ vs. B-V color index is empty. This suggests that the dwarf stars are not decelerated beyond a maximum rotation period depending on the spectral type. The maximum period is larger for cooler stars.

The spin-down law (1.3) applies to the solar-type stars over a major part of their main-sequence life. Gray (1982) and Rengarajan (1984) forwarded the idea that the proportionality constant in the relation (1.3) is a single-valued function of stellar mass or other equivalent parameter. This idea eventually led to the development of gyrochronology establishing an empirical relation between age, rotation period and mass (Barnes, 2003, 2007, 2010; Collier Cameron *et al.*, 2009; Meibom, Mathieu,

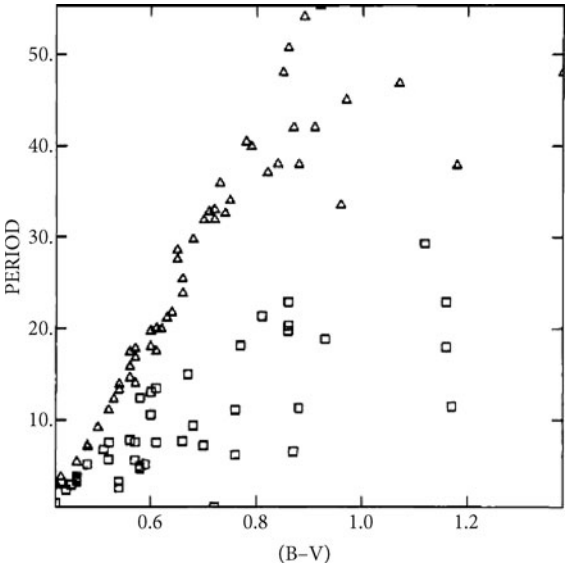

Figure 1.8 Plot of P_{rot} (in days) versus B-V color for main-sequence stars. The squares and triangles refer to young and old stars, respectively. From Rengarajan (1984). Reprinted by permission of AAS.

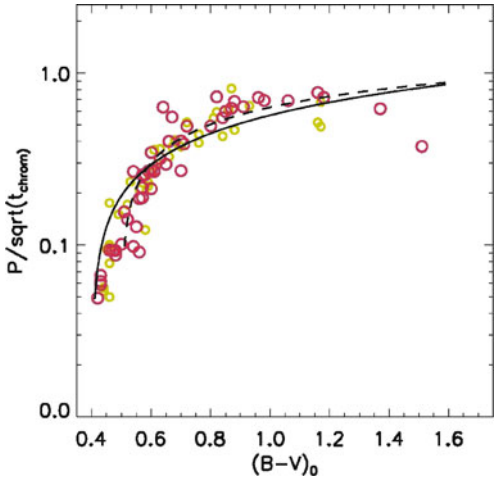

Figure 1.9 The ratio of P_{rot} (days) to square root of t (Myr) in dependence on B-V color for main-sequence stars of the Mount Wilson sample. Small and large circles show young and old stars, respectively. From Barnes (2007). Reprinted by permission of AAS.

and Stassun, 2009). The relation is illustrated by Figure 1.9 where the dependence of the ratio $P_{rot}/\sqrt{t}$ on B-V color is shown. Different functional expressions for the

empirical relation have been suggested, for example

$$P_{\mathrm{rot}} = a t^{n} \, (\mathrm{B} - \mathrm{V} - c)^{b} \tag{1.4}$$

in days with $n = 0.519 \pm 0.007$, $a = 0.773 \pm 0.011$, $b = 0.601 \pm 0.024$, $c = 0.4$, where t is measured in Myr (Barnes, 2007). The characteristic error of this relation when applied to gigayear-old stars from early M to late F is reported as within 20%.

1.2.2 Differential Rotation

Stellar differential rotation is measured mainly by the same method, which originally was used for the Sun, that is, by tracing the rotation of thermal or magnetic spots. As stars are typically point sources (only in very rare, exceptional cases can stellar surfaces be resolved), the methods are very sophisticated and demanding of observational data. The tracer method can be realized using high precision (space-based) photometry or high resolution spectroscopy with the Doppler imaging techniques. The differential rotation was also measured using shapes of spectral lines (Reiners and Schmitt, 2003a,b) and variations of Ca II H&K emissio (e.g., Donahue, Saar, and Baliunas, 1996). Doppler imaging (Khokhlova, 1975; Vogt and Penrod, 1983) provides detailed mapping of stellar surfaces but can be used only for young rapidly rotating stars because the projected rotation velocity $v \sin i$ should typically not be smaller than 15 km/s. Measurements of differential rotation by Doppler imaging were summarized by Barnes *et al.* (2005) to reveal strong dependence on spectral type: the hotter the star, the larger the pole–equator difference in rotation

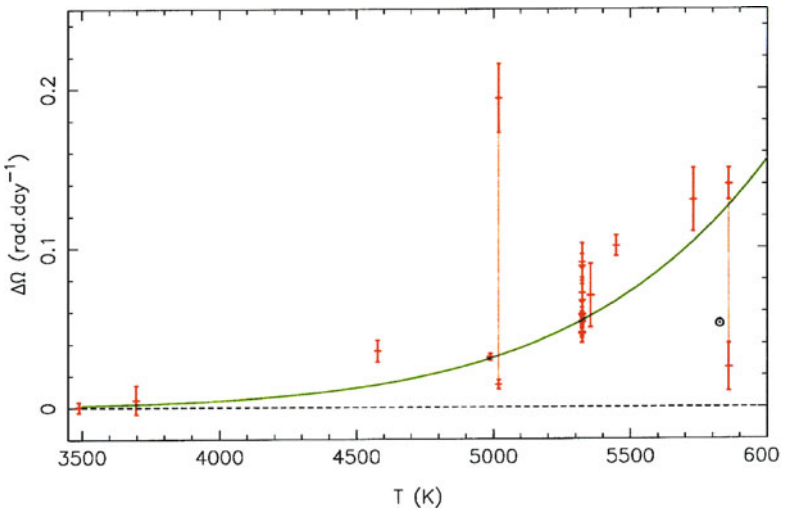

Figure 1.10 Dependence of surface differential rotation on effective temperature for rapidly rotating solar analogs by Doppler imaging (Barnes *et al.*, 2005). Copyright © 2005 RAS.

rate. Observed differential rotation is usually fit by the $\sin^2 b$ profile

$$\Omega = \Omega_{\rm eq} - \delta\Omega \sin^2 b \, . \tag{1.5}$$

Figure 1.10 shows the pole–equator difference $\delta\Omega$ as a function of temperature for young solar-type stars. The largest differential rotation belongs to the hottest stars. Jeffers and Donati (2008) found the slightly premain-sequence G0 star HD 171488 (V889 Her) with $\delta\Omega \simeq 0.5$ rad/day exceeding all stars of Figure 1.10 in magnitude of its differential rotation (see Section 1.6.2).

The dependence of $\delta\Omega$ on the rotation rate is probably mild. The very rapidly rotating ($P_{\rm rot} = 0.51$ day) solar analog AB Dor possesses almost the same differential rotation as the Sun (Donati and Collier Cameron, 1997). Figure 1.11 shows differential rotation of several stars close to the Sun by mass but rotating with different rates. Rotation of the stars with $P_{\rm rot} < 2$ days of this figure was defined by Doppler imaging. For the slowest rotator in this sample, LQ Hya, large variations with time has been seen by Donati *et al.* (2003). Differential rotation of two moderate rotators, κ^1 Ceti and ε Eri, was measured using high precision photometry of the MOST mission (Croll *et al.*, 2006; Walker *et al.*, 2007). The stars of Figure 1.11 spanning almost two orders of magnitude in rotation rate show a very similar amount of differential rotation. This suggests that absolute value of differential rotation varies mainly with stellar surface temperature, variation with rotation rate being mild.

When common statistics for stars of different spectral types is used, however, an increase of differential rotation with rotation rate is usually found (cf. Donahue, Saar, and Baliunas (1996)). As can be seen from Figure 1.8 or the gyrochronology equation (1.4), slow rotators are mainly represented by K stars while G and F stars

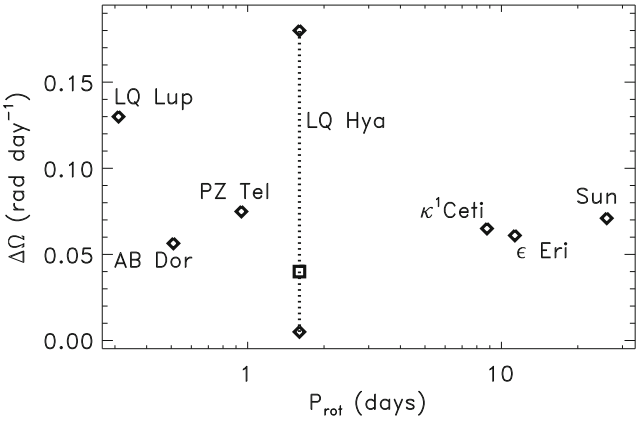

Figure 1.11 Observed differential rotation of stars close to the Sun by mass but rotating with different rates. LQ Lup is a premain-sequence star (Donati *et al.*, 2000). AB Dor (Donati and Collier Cameron, 1997), PZ Tel (Barnes *et al.*, 2000) and LQ Hya (Donati *et al.*, 2003) are ZAMS stars. Flores-Soriano and Strassmeier (2013) give $\delta\Omega \simeq 0.04$ rad/day for LQ Hya. Differential rotation of these stars was measured by Doppler imaging. High-precision photometry of the MOST mission was used for older stars ε Eri (Croll *et al.*, 2006) and κ^1 Ceti (Walker *et al.*, 2007).

show much shorter rotation periods. The increase of differential rotation with rotation rate is found because rotation of cooler stars is more uniform (Figure 1.10).

The primary chromospherically active stars of the close RS CVn binary systems seem to show a more complicated behavior. Kővári *et al.* (2012) report for ζ And the characteristic value $\delta\Omega = 0.02$ rad/day. Another example is the highly active K2 giant II Peg with its mass of 0.8 $M_\odot$ and the rotation period of 6.72 days. Henry *et al.* (1995) report a very weak solar-type rotation law with $\delta\Omega \simeq 0.005$ rad/day while Siwak *et al.* (2010) derive the much higher value $\delta\Omega \simeq 0.023$ rad/day from Mosт data. Roettenbacher *et al.* (2011) basically confirm the small value of Henry *et al.* (1995). Weber and Strassmeier (2005) yield with $\delta\Omega \simeq 0.04$ rad/day an even higher value. They also showed that in their sample single stars exhibit significantly higher values of $\delta\Omega$ than members of binaries (Figure 9 in Weber and Strassmeier (2005)). It is insofar interesting that Oláh *et al.* (2013) find the small but similar values $\delta\Omega \simeq 0.006$ rad/day for V2253 ($P_{\rm rot} = 21.55$ days) and $\delta\Omega \simeq 0.007$ rad/day for IT Com ($P_{\rm rot} = 65.1$ days).

For the very young T Tau stars the early investigations led to almost solid-body rotation. Rice and Strassmeier (1996) found only a ratio $\delta\Omega/\Omega \simeq 0.001$ for V410 Tau with its rotation period of 1.87 days. The equator–pole difference results in the positive but small value $\delta\Omega \simeq 0.0035$ rad/day. In a recent analysis of Mosт data Siwak *et al.* (2011) confirmed the smallness of this value ($\delta\Omega \simeq 0.002$ rad/day) but for two other weak-line TTS the values $\delta\Omega \simeq 0.026$ rad/day and $\delta\Omega \simeq 0.045$ rad/day have been found which do not confirm the solid-body hypothesis.

1.3 The Reynolds Stress

The theory of differential rotation is mainly the theory of angular momentum transport. The angular momentum equation for a turbulent rotating fluid reads as

$$\frac{\partial}{\partial t}(\rho R^2 \Omega) = -\nabla \cdot \left\{ \rho R \langle u_\phi \boldsymbol{u} \rangle + \rho R^2 \Omega \, \boldsymbol{U}^{\rm m} - \frac{R}{\mu_0} \left[\bar{B}_\phi \bar{\boldsymbol{B}} + \langle b_\phi \boldsymbol{b} \rangle \right] \right\} , \quad (1.6)$$

where $R = r \sin\theta$ is the distance to the rotation axis, $\bar{\boldsymbol{U}}$ and $\bar{\boldsymbol{B}}$ are the mean flow and the mean magnetic field, $\boldsymbol{u}$ and $\boldsymbol{b}$ are their fluctuating parts, $\boldsymbol{U}^{\rm m}$ is the meridional flow, and angular brackets signify the averaging over an ensemble of realizations of turbulence. The vector in curly brackets of (1.6) is the angular momentum flux. The angular momentum can be transported by turbulence, global meridional flow and by magnetic stress.

Turbulence is well known to be capable of transporting momentum by the effect of turbulent viscosity. Turbulent mixing smooths out the mean velocity shear. This turbulent viscosity effect can only bring a star to the state of uniform rotation. It has been found, however, that rotating turbulence can transport angular momentum even in a state of rigid rotation. This nondiffusive transport, named

the Λ effect (Rüdiger, 1989), is of key importance for understanding differential rotation of convective stars.

1.3.1 The Λ Effect

The pseudovector of angular velocity alone does not suffice to construct a polar vector of angular momentum flux. The turbulent fluid, therefore, has to possess a preferred direction for the Λ effect to emerge (Lebedinskii, 1941; Biermann, 1951). The preferred direction in stellar convection zones is provided by gravity.

The physical origin of the Λ effect is illustrated by Figure 1.12. The dashed arrows show the original motions and the solid arrows show the motions perturbed by the Coriolis force. A fluid particle, which moves originally in radius, attains azimuthal velocity, which can be estimated as $u_\phi \simeq -2\tau_{\rm corr}\Omega\, u_r \sin\theta$, where $\tau_{\rm corr}$ is the characteristic time of turbulent mixing. The product $u_r u_\phi \simeq -2\tau_{\rm corr}\Omega\, u_r^2 \sin\theta$ is negative independently of whether the original radial motion is upward or downward. For an original azimuthal motion, radial velocity $u_r \simeq 2\tau_{\rm corr}\Omega\, u_\phi \sin\theta$ is produced by the Coriolis force, and the product $u_r u_\phi \simeq 2\tau_{\rm corr}\Omega\, u_\phi^2 \sin\theta$ is positive. On average, we have

$$\langle u_r u_\phi\rangle \simeq 2\tau_{\rm corr}\Omega \left(\langle u_\phi^2\rangle - \langle u_r^2\rangle\right)\sin\theta\ ,$$
$$\langle u_\theta u_\phi\rangle \simeq 2\tau_{\rm corr}\Omega \left(\langle u_\phi^2\rangle - \langle u_\theta^2\rangle\right)\cos\theta\ .$$

Anisotropy of turbulence with different intensity of radial and horizontal mixing is required for the net radial flux of angular momentum to arise. A latitudinal flux of angular momentum results if the two components of the horizontal turbulence intensities differ. It thus makes sense to introduce the anisotropy parameters $A_{\rm V} = \langle u_\phi^2 - u_r^2\rangle/u_{\rm rms}^2$ and $A_{\rm H} = \langle u_\phi^2 - u_\theta^2\rangle/u_{\rm rms}^2$ so that $Q_{r\phi} \propto A_{\rm V}$ and $Q_{\theta\phi} \propto A_{\rm H}$ results.

The above expressions for the cross-correlation involve the Coriolis number

$$\Omega^* = 2\tau_{\rm corr}\Omega \tag{1.7}$$

as a key parameter of the differential rotation theory. This parameter measures the intensity of interaction between convection and rotation. Its value defines whether turbulent eddies are long-lived enough for rotation to significantly influence them. The Coriolis number is reciprocal to another commonly used Rossby number Ro =

Figure 1.12 Illustration of angular momentum transport by rotating turbulence. The direction of rotation is shown at the top. See text.

$P_{\rm rot}/\tau_{\rm corr}$, that is, $\Omega^* = 4\pi {\rm Ro}^{-1}$. The Coriolis number depends on depth in a stellar convection zone. Figure 1.14a shows its depth profile for the Sun. Ω^* exceeds unity in the major part of the convection zone. This condition of strong interaction between convection and rotation, $\Omega^* > 1$, which is typical of solar-type stars, largely complicates the Λ effect theory. It means that the above linear estimates no longer apply, and a better theory should be fully nonlinear in rotation rate.

1.3.1.1 Numerical Simulations

Käpylä and Brandenburg (2008) simulated with the Pencil Code homogeneous but anisotropic turbulence by use of variable anisotropic forcing functions in boxes with 256^3 grid points. In all simulations the radial velocity fluctuations dominated the other components so that always $A_{\rm V} < 0$. Without rotation both the horizontal velocity intensities are equal. The global rotation suppresses the vertical turbulence and increases the horizontal rms values. By this influence the (negative) $A_{\rm V}$ is reduced and a small but positive $A_{\rm H}$ results so that a negative radial angular momentum flux and a positive horizontal angular momentum flux can be expected. Because of the rotational isotropizing of the turbulence a sufficiently rapid rotation should remarkably quench the two components of the angular momentum flux (radial and latitudinal). Figure 1.13a shows the calculated off-diagonal elements of the Reynolds stress tensor. Indeed, the resulting $Q_{r\phi}$ is negative while the result-

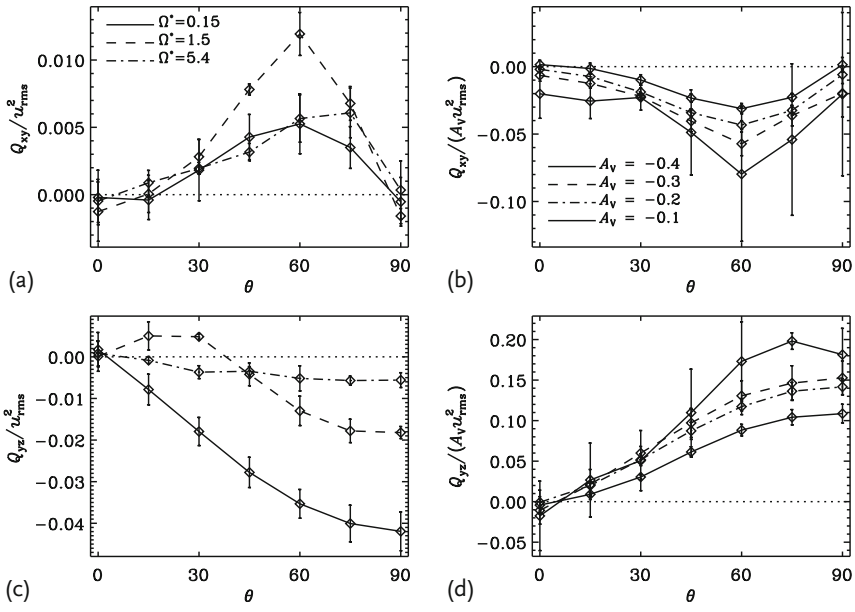

Figure 1.13 The Λ effect of turbulence due to anisotropic forcing. The numerical values are also the cross-correlation coefficients. (a,c) The off-diagonal elements of the normalized Reynolds tensor $Q_{ij}/u_{\rm rms}^2$ vs. the colatitude. (a,b) $Q_{\theta\phi}$ and (c,d) $Q_{r\phi}$. (b,d) The same but for $Q_{\theta\phi}/(A_{\rm V}u_{\rm rms}^2)$ and $Q_{r\phi}/(A_{\rm V}u_{\rm rms}^2)$. The Coriolis number is fixed. From Käpylä and Brandenburg (2008). Reproduced with permission © ESO.

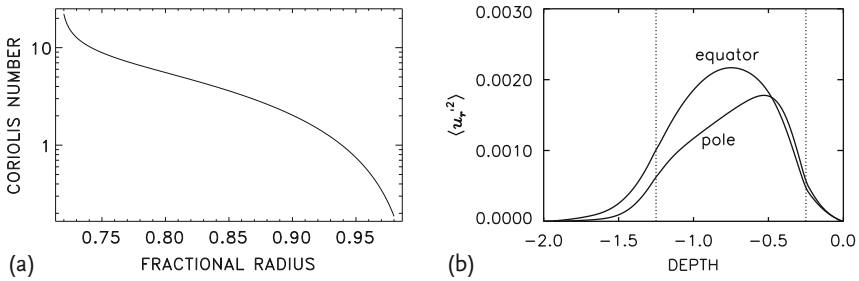

Figure 1.14 Depth profile of the Coriolis number (1.7) in the solar convection zone according to the solar structure model by Stix and Skaley (1990) (a). Shown also is the radial turbulence intensity for Ta $= 10^6$ (b). The flow amplitudes are normalized with the sound velocity at the surface of the unstable domain.

ing $Q_{\theta\phi}$ is positive (but small). That the radial transport of the angular momentum is indeed due to the radial anisotropy of the turbulence can be demonstrated with Figure 1.13b. There the ratio $Q_{r\phi}/A_{\rm V}$ is shown as almost independent of the numerical value of the turbulence field considered.

The anisotropy in solar and stellar convection zones can be studied in detail with 3D simulations of thermal convection (Pulkkinen *et al.*, 1993; Chan, 2001; Käpylä, Korpi, and Tuominen, 2004; Rüdiger, Egorov, and Ziegler, 2005). In the following representation of numerical simulations with the Nirvana Code the Λ effect is renormalized in accordance to

$$\Lambda_{\rm V}^* = \frac{\Lambda_{\rm V}\Omega}{c_{\rm ac}^2}\,, \quad \Lambda_{\rm H}^* = \frac{\Lambda_{\rm H}\Omega}{c_{\rm ac}^2} \tag{1.8}$$

so that

$$V = \Lambda_{\rm V}^* \frac{c_{\rm ac}^2}{\nu_{\rm T}\Omega}\,, \quad H = \Lambda_{\rm H}^* \frac{c_{\rm ac}^2}{\nu_{\rm T}\Omega}\,. \tag{1.9}$$

For the Sun the value of $c_{\rm ac}^2/(\nu_{\rm T}\Omega)$ is of order 10^4. In order to get V and/or H of order unity the simulations for Λ^* should yield rather small values. In the calculations Ra $= 3 \times 10^5$ and Pr $= 0.1$, while Ta varies from 10^4 to 10^6 which may represent the realization of slow rotation and fast rotation. The value Ta $= 10^6$ does not describe the real solar convection but it seems to be large enough to reveal the relation between anisotropy and angular momentum transport in rotating convection. All velocities are normalized with the speed of sound ($c_{\rm ac}$) at the upper layer of the unstable domain. Its solar value is about 6.4 km/s. In Figure 1.14 the maximum velocity in the box is given with 0.044, which would mean about 300 m/s for the solar case. This value corresponds to the velocity amplitudes which are characteristic in the bulk of the solar convection zone. Figure 1.14b also reveals that for Ta $= 10^6$ the turbulence intensity $\langle u_r^2\rangle$ grows from the pole to the equator. This unexpected result for rapid rotation is also present in the simulations of convection in boxes with weak density stratification (Chan, 2001; Käpylä and Brandenburg, 2008; Snellman *et al.*, 2009).

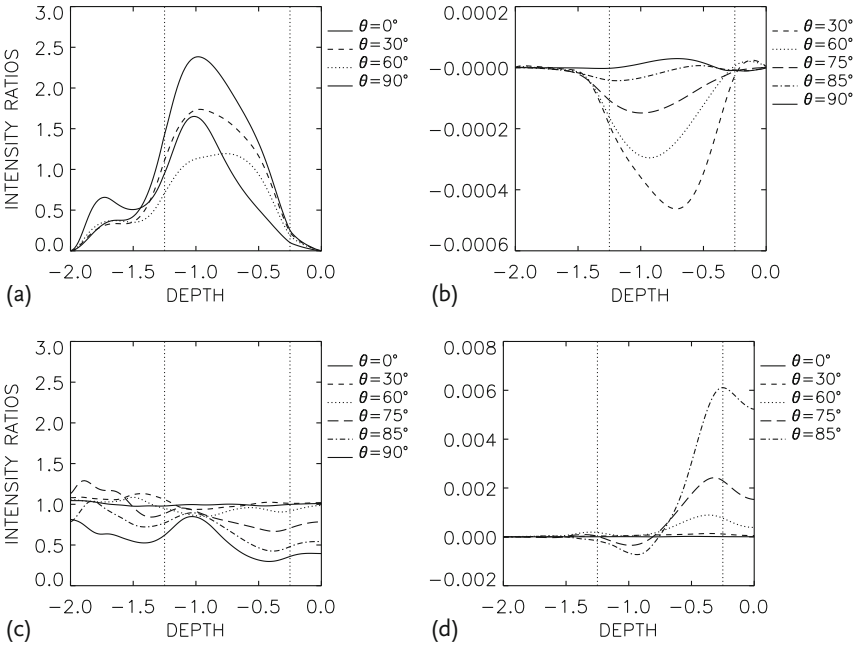

Figure 1.15 The ratio $\langle u_r^2 \rangle / \langle u_\phi^2 \rangle$ of the turbulence intensities for rotating turbulence fields (a), the function Λ_V^*. Ta $= 10^6$ (b), and the intensity ratio $\langle u_\theta^2 \rangle / \langle u_\phi^2 \rangle$ (c). Note the dominance of $\langle u_\phi^2 \rangle$. The function Λ_H^* is basically positive (d). Ta $= 10^6$. The instability domain is located between the two vertical lines in each plot. From Rüdiger *et al.* (2005a).

The anisotropy between vertical and azimuthal turbulence intensities is shown in Figure 1.15a. Without rotation the turbulence is vertically dominated except in the top layer. This is also true for the lower overshoot zone between the unstable and the stable layer ('tachocline'). We therefore expect the occurrence of negative Λ_V in the bulk of the convection zone.

For Ta $= 10^4$ the resulting Λ_V is small. Already for Ta $= 10^6$, however, the results are very clear (Figure 1.15b). The function Λ_V^* is zero at the equator and is negative in both hemispheres (see Chan, 2001). The vanishing of Λ_V^* at the equator is not trivial and requires formulations such as $Q_{r\phi} \propto \cos^{2l}\theta \sin\theta$ with $l > 0$. Note also that the Λ_V^* vanishes in the upper overshoot layer while it remains basically negative in the tachocline layer.

The amplitude of Λ_V^* for Ta $= 10^6$ is 4×10^{-4} which leads to $V \simeq 10$. The behavior of the anisotropy parameter $\langle u_r^2 \rangle / \langle u_\phi^2 \rangle$ for rapid rotation is of particular interest. At the poles the influence of the rotation is rather small. It is much stronger in the equatorial region. There, we find a tendency of return-to-isotropy as a consequence of the Taylor–Proudman theorem. A possible vanishing of the radial angular momentum transport at the equator might be due to this phenomenon.

The horizontal angular momentum transport is based on the anisotropy in the turbulence field between both the horizontal components which only exists for rotating stars (Figure 1.15c). It is therefore not surprising that in contrast to the

radial angular momentum transport, for rapid rotation (Ta $= 10^6$) only, a remarkable effect exists. The anisotropy in the turbulence field between $\langle u_\phi^2 \rangle$ and $\langle u_\theta^2 \rangle$ exists mainly in the equatorial region. There $\langle u_\phi^2 \rangle$ dominates, leading to positive cross-correlations close to the equator, that is $\Lambda_{\rm H}^* > 0$ (Figure 1.15d).

The amplitude of $Q_{\theta\phi}$ is greater than the amplitude of $Q_{r\phi}$, and is positive in the upper half of the convection zone. The amplitude of H, therefore, exceeds the amplitude of V by a factor of about 10 – similar to Chan's results obtained with a completely different code. In the lower half of the convective domain it is much smaller and negative and also highly concentrated at the equator.

The situation in the lower overshoot region is also of interest. Note that the turbulence in both (rotating) overshoot regions is horizontal rather than vertical, that is $A_{\rm V} > 0$. At the top of the convection box the situation is more complicated. For slow rotation (Ta $= 10^5$) there is no H but a negative V which only depends slightly on the latitude. The same is true for the negative slope of the outer solar rotation law in the supergranulation layer (see Figure 1.1). For faster rotation (Ta $= 10^6$) one finds the opposite. V goes to zero and H is a positive and large number (in the equatorial region). This is a basic problem existing in the entire box.

Motivated by this problem, and in order to avoid possible numerical artifacts of box simulations, Käpylä *et al.* (2011) designed global simulations in a 'wedge' geometry defined by $0.65 \le x \le 1$, $15^\circ \le \theta \le 165^\circ$ and $0 \le \phi \le 90^\circ$. For the thermal stratification a piecewise polytrophic setup is used with the logarithmic temperature gradient $\nabla = \partial \log T / \partial \log P = 1/(n+1)$ which describes an unstable domain for $n < 1.5$. This convection zone has been sandwiched by two stable overshoot regions. The radial and latitudinal boundaries are taken to be impenetrable and stress-free, and the heat-fluxes are suppressed through the latitudinal boundaries. The simulations were performed with the Pencil Code code in spherical coordinates (for details see Mitra *et al.*, 2009).

The results have been obtained with fixed low Mach number but with a free Coriolis number of order unity. The latter is insofar important as the wanted off-diagonal elements of the Reynolds stress tensor only exist for sufficiently rapid rotation. Figure 1.16 presents the resulting radial flux of angular momentum $Q_{r\phi}$ normalized with the turbulence intensity $u_{\rm rms} = \sqrt{\langle u_r^2 + u_\theta^2 \rangle}$. Indeed, there is almost no signal for the two lowest Ω^* (Figure 1.16a,b). For the intermediate rotation rates symmetric profiles with respect to the equator appear with predominantly negative signs confirming the basic result of the above presented box simulations. For the fastest rotation with $\Omega^* \simeq 6$, $Q_{r\phi}$ becomes smaller and even positive.

As it should, the signals for the latitudinal flux of angular momentum are antisymmetric with respect to the equator with positive values at the northern hemisphere so that the angular momentum is transported from the poles to the equator (Figure 1.17). For the fastest rotation with $\Omega^* \simeq 6$ the cross-correlation values at the top and bottom of the convection zone are rotationally quenched. The striking maxima very close to the equator which are characteristic for the box simulations (see also Hupfer, Käpylä, and Stix, 2005, 2006) no longer appear in the global simulations.